A comparison between different numerical methods for the modeling of polycrystalline materials with an elastic-viscoplastic behavior

Camille Robert[a], Charles Mareau[a]

[a] *Arts et Métiers ParisTech, Campus d'Angers, LAMPA, 2 bd du Ronceray, 49035 Angers Cedex 1, France*

Abstract

The macroscopic behavior of polycrystalline materials is largely influenced by the shape, the arrangement and the orientation of crystallites. Different methods have thus been developed to determine the effective behavior of such materials as a function of their microstructural features. In this work, which focuses on polycrystalline materials with an elastic-viscoplastic behavior, the self-consistent, finite element and spectral methods are compared. These common methods are used to determine the effective behavior of different 316L polycrystalline aggregates subjected to various loading conditions. Though no major difference is observed at the macroscopic scale, the hardening rate is found to be slightly overestimated with the finite element method. Indeed, spatial convergence cannot be guaranteed for finite element calculations, even when fine mesh resolutions, for which the computational cost is important, are used. Also, as the self-consistent method does not explicitly account for neighborhood effects, important discrepancies between the self-consistent method and the other methods exist regarding the mechanical response of a specific grain. The self-consistent method nevertheless provides a reasonable description of the average response obtained for a group of grains with identical features (e.g. shape, orientation).

Keywords: Homogenization, Elasto-viscoplasticity, Self-consistent method, Finite element method, Spectral method, Heterogeneous materials

1. Introduction

The behavior of engineering materials is sometimes better described by accounting for the heterogeneous aspect of the strain and stress fields which develop during a deformation process. For the specific case of polycrystalline materials, the main reason for the fluctuations of the strain and stress fields

Email addresses: camille.robert@ensam.eu (Camille Robert), charles.mareau@ensam.eu (Charles Mareau)

is the anisotropy of single crystal elastic and plastic properties. These fluctuations, which may significantly impact the effective behavior of a polycrystalline aggregate, depend on the properties, the shape, the arrangement and the orientation of the different crystallites. Different methods have thus been developed to account for the polycrystalline nature of such materials when determining the effective properties.

Historically speaking, the first propositions were made by Hershey [1] and Kröner [2] who developed the self-consistent scheme to estimate the effective properties of heterogeneous materials. Since the initial propositions of Hershey [1] and Kröner [2] are restricted to constitutive models with a linear form (e.g. linear elasticity, newtonian viscosity), different extensions have been proposed to deal with heterogeneous materials with non-linear constitutive relations. For instance, the developments made by Kröner [3] and Hill [4] allow for modeling the behavior of heterogeneous materials for which the constitutive relation includes both elasticity and rate-independent plasticity. Neglecting elastic contributions, Hutchinson [5], Molinari et al. [6] and Lebensohn and Tomé [7] adapted the self-consistent model to the case of heterogeneous solids with a viscoplastic behavior. When dealing with elastic-viscoplastic constitutive relations, additional difficulties exist because constitutive relations involve different orders of time derivation. Indeed, complex space-time couplings, described by Suquet [8] as the long-memory effect, are involved and the local and macroscopic constitutive models do not have the same structure anymore. To overcome these difficulties, many approaches have been proposed. They fall into two different categories. On the one hand, hereditary models use Laplace-Carson transforms to define a single viscoelastic modulus in the Laplace-Carson space [9, 10, 11, 12]. The self-consistent problem can then be solved in the Laplace-Carson space before proceeding to the inversion of the solution to the real time space. On the other hand, interval variable models are entirely formulated in the real-time space [13, 14, 15, 16, 17, 18, 19, 20]. They are based on a set of internal variables whose introduction allows accounting for the interactions associated with the space-time couplings.

The finite element method [21, 22, 23] is commonly used for the resolution of mechanical engineering problems. As shown by the pioneering work of Miyamoto et al. [24], the finite element method is a convenient way of investigating the local behavior of crystalline materials. Indeed, in contrast with the self-consistent method, the finite element method aims at providing stress and strain fields for which compatibility and static equilibrium conditions are locally fulfilled. The finite element method thus allows for capturing the intragranular fluctuations of the stress and strain fields. As a result, thanks to the development of computing capabilities, there has been a growing interest for the numerical simulation of polycrystalline aggregates with the finite element method [25, 26, 27, 28, 29, 30, 31, 32].

The spectral method proposed by Moulinec and Suquet [33] is an alternative solution for the modeling of heterogeneous materials. It makes an intensive use of the Fast Fourier Transform algorithm to solve the integral equation associated with the heterogeneous problem. Though the initial applications of Moulinec

and Suquet [33] were focused on composite materials, different extensions have been developed in the context of crystal plasticity [34, 35, 36, 37]. In contrast with the finite element method, the periodicity of both the microstructure and the boundary conditions is a necessary condition for the application of the spectral method.

Because of their design, the self-consistent, finite element and spectral methods are based on different assumptions. As a result, the choice of an appropriate method for a given problem requires being aware of how these assumptions may influence the estimate of effective properties. The present work thus aims at comparing these methods in the context of the determination of the effective properties of polycrystalline aggregates with an elastic-viscoplastic behavior. The paper is structured as follows. In the first part, the equations associated with the heterogeneous problem are presented and the different methods are briefly described. In the second part, some applications are proposed and the results determined with the different methods are compared. The results are obtained for 316L polycrystalline aggregates subjected to different loading conditions: uniaxial tension, cyclic tension-compression and some multiaxial loading paths allowing for the determination of yield surfaces.

2. Model description

2.1. Field equations

In this work, a volume element V with boundary ∂V, which is representative of a polycrystalline material, is considered. The volume element consists of many subdomains with homogeneous properties (i.e. crystallites) being perfectly bonded across their interfaces. The effective properties are determined from the macroscopic stress and strain tensors (denoted by Σ and E) which are related to the local stress and strain fields (denoted by σ and ε) through the classical averaging relations of homogenization theory:[1]

$$\Sigma(t) = \frac{1}{V}\int_V \sigma(x,t)\, dV = <\sigma(t)>_V \tag{1}$$

$$E(t) = \frac{1}{V}\int_V \varepsilon(x,t)\, dV = <\varepsilon(t)>_V \tag{2}$$

Within the infinitesimal strain framework, kinematical compatibility relations are given at any point x and any time t by:

$$\varepsilon(x,t) = \mathrm{sym}\left(u(t) \otimes \nabla_x\right) \tag{3}$$

$$\dot{\varepsilon}(x,t) = \mathrm{sym}\left(\dot{u}(t) \otimes \nabla_x\right) \tag{4}$$

[1] These relations hold if and only if the volume element is submitted to homogeneous boundary conditions or periodic boundary conditions. Only these specific (but rather common) situations are considered in the present work.

where u is the displacement field. Also, when no volume forces are present, the stress field σ should satisfy the static equilibrium conditions:

$$\nabla_x \cdot \sigma(t) = 0 \tag{5}$$

$$\nabla_x \cdot \dot{\sigma}(t) = 0 \tag{6}$$

Assuming an elastic-viscoplastic behavior, the local strain and strain rate fields are decomposed into elastic (subscript e) and viscoplastic (subscript p) contributions:

$$\varepsilon(x,t) = \varepsilon_e(x,t) + \varepsilon_p(x,t) \tag{7}$$

$$\dot{\varepsilon}(x,t) = \dot{\varepsilon}_e(x,t) + \dot{\varepsilon}_p(x,t) \tag{8}$$

Within a rate-dependent framework, the viscoplastic strain rate $\dot{\varepsilon}_p$ is a non-linear function f of the stress tensor σ and some internal variables v_k whose detail does not need to be known at this stage:

$$\dot{\varepsilon}_p(x,t) = f(\sigma, v_k) \tag{9}$$

The introduction of the elastic stiffness tensor c allows for connecting the stress and stress rate tensors to the strain and strain rate tensors:

$$\sigma(x,t) = c(x) : (\varepsilon(x,t) - \varepsilon_p(x,t)) \tag{10}$$

$$\dot{\sigma}(x,t) = c(x) : (\dot{\varepsilon}(x,t) - \dot{\varepsilon}_p(x,t)) \tag{11}$$

In order to close the above problem, which consists of equations (3) to (11), the boundary conditions have to be specified. The boundary conditions prescribed on ∂V should reflect as better as possible the in-situ state of the representative volume element. However, in most cases, only partial information regarding the exact in-situ state is available. Therefore, depending on the method, different strategies have been adopted to circumvent this difficulty.

In the general case, no analytical solution exists for the heterogeneous problem which is uniquely defined from field equations and boundary conditions. Consequently, different methods, which are briefly described in the following sections, have been developed to obtain numerical solutions to this problem. These methods aim at finding the stress and strain fields (or equivalently the stress rate and strain rate fields) satisfying both compatibility, equilibrium and boundary conditions.

In the following, unless otherwise specified, the dependence with time t and position x will be omitted.

2.2. Finite element method

The finite element method aims at finding approximate solutions to boundary value problems such as the heterogeneous problem described earlier. The first step consists of writing the heterogeneous problem in its weak form. The

weak formulation is obtained by introducing a virtual displacement field v which allows for transforming equation (5) into:

$$\int_V (\nabla_x \cdot \sigma) \cdot v \, dV = 0 \tag{12}$$

Integrating by parts the above relation and using the divergence theorem leads to the weak formulation of the heterogeneous problem:

$$\int_V \sigma : \epsilon \, dV - \int_{\partial V} (\sigma \cdot n) \cdot v \, dS = 0 = R(u) \tag{13}$$

where n is the unit normal vector associated with the boundary ∂V and ϵ is the compatible strain field deriving from v (i.e. $\epsilon = \mathrm{sym}(v \otimes \nabla_x)$). In the present case, periodic boundary conditions are imposed to the representative volume element. For this particular situation, the displacement fields (u and v) are decomposed into linear ($E \cdot x$) and periodic ($\tilde{u}$ and $\tilde{v}$) parts:

$$u = E \cdot x + \tilde{u} \tag{14}$$

$$v = E \cdot x + \tilde{v} \tag{15}$$

Thus, if the virtual displacement field v is chosen to vanish on ∂V, the weak formulation (13) reduces to:

$$\int_V \sigma : \epsilon \, dV = R(u) \tag{16}$$

The finite element method consists of discretizing the representative volume element in subdomains (finite elements) for which the geometry and the displacement fields are approximated with shape functions. In the present case, isoparametric finite elements (i.e. with identical functions for both the geometry and the displacement field) are used. The introduction of the shape functions N^n, for which local support is assumed, allows for expressing the displacement fields u and v for any point as a function of the nodal displacement vectors U and V:

$$u = N^n \cdot U \tag{17}$$

$$v = N^n \cdot V \tag{18}$$

The periodic boundary conditions are imposed according to the procedure proposed by Dirrenberger [38] which consists in adding global degrees of freedom for the prescription of the macroscopic strain tensor E. Indeed, using the above relations and under the assumption of periodic boundary conditions, the strain tensors ε and ϵ are given by:

$$\varepsilon = \mathrm{sym}\left(\left(N^n \cdot \tilde{U}\right) \otimes \nabla_x\right) + E = B^n \cdot U' \tag{19}$$

$$\epsilon = \mathrm{sym}\left(\left(N^n \cdot \tilde{V}\right) \otimes \nabla_x\right) + E = B^n \cdot V' \tag{20}$$

The vectors U' and V' are obtained by concatenating the unknown nodal periodic displacement vectors $\tilde{U}$ and $\tilde{V}$ and the prescribed macroscopic strain tensor E. According to the above expressions of the strain tensors, relation (16) becomes:

$$\int_V \sigma : (B^n \cdot V')\, dV = R(u) \tag{21}$$

Since the constitutive relation (10) is non-linear, the resolution of the above problem, for which the solution is given by the unknown vector U', necessitates a numerical procedure for the minimization of R. An iterative Newton-Raphson procedure is used here. Thus, with a given estimate of U' (iteration i), a new estimate (iteration $i+1$) is calculated from:

$$\left.\frac{\partial R}{\partial U'}\right|_i \cdot \left(U'_{i+1} - U'_i\right) = -R(u_i) \tag{22}$$

The differentiation of R regarding U' is given by:

$$\frac{\partial R}{\partial U'} = \int_V \frac{\partial \varepsilon}{\partial U'} : \frac{\partial \sigma}{\partial \varepsilon} : \epsilon\, dV = \int_V {B^n}^T : \frac{\partial \sigma}{\partial \varepsilon} : B^n \cdot V'\, dV \tag{23}$$

This procedure, which is repeated until convergence is achieved, allows for solving the non-linear equation (21). Classically, the convergence criterion is based on the evaluation of the residual nodal forces which are required to be inferior to a certain tolerance e:

$$\frac{\left|\left|\int_V \sigma : B^n\, dV - \int_V {B^n}^T : \frac{\partial \sigma}{\partial \varepsilon} : B^n \cdot U'\, dV\right|\right|}{\left|\left|\int_V {B^n}^T : \frac{\partial \sigma}{\partial \varepsilon} : B^n \cdot U'\, dV\right|\right|} \leq e \tag{24}$$

Knowing the nodal displacement vector at a given time t, the strain field can be determined for any point x with relation (19). The stress field is then calculated by integrating the constitutive relation (10).

2.3. Spectral method

The spectral method, which was first introduced by Müller [39] and Moulinec and Suquet [33], requires discretizing the representative volume element into voxels. The application of the spectral method necessitates both the microstructure and the boundary conditions to be periodic. The boundary conditions are thus given by relation (14). The spectral method uses the Fast Fourier Transform (FFT) algorithm to find a numerical solution to the integral equation associated with the heterogeneous problem. To obtain the integral equation, the local elastic modulus c is expressed as the sum of a uniform reference modulus C and a fluctuating part δc:

$$c(x) = C + \delta c(x) \tag{25}$$

According to the above decomposition, the local constitutive law (10) can be written:

$$\sigma = C : \varepsilon + \tau \tag{26}$$

where τ is the polarization field defined by:

$$\tau = \delta c : \varepsilon - c : \varepsilon_p \tag{27}$$

The integral equation is obtained by introducing the modified Green operator Γ^C associated with the reference medium in equation (26). The modified Green operator Γ^C display specific properties for any compatible field (like ε) and any balanced field (like σ):

$$\left(\Gamma^C : C\right) * \varepsilon = \varepsilon - E \tag{28}$$

$$\Gamma^C * \sigma = 0 \tag{29}$$

where $*$ denotes the spatial convolution product. The introduction of the modified Green operator Γ^C in relation (26) leads to the following periodic Lippmann-Schwinger integral equation:

$$\varepsilon = E - \Gamma^C * \tau \tag{30}$$

The application of the Fourier transform converts the integral equation from the spatial domain to the frequency domain according to:

$$\hat{\varepsilon}\left(\xi, t\right) = \begin{cases} E\left(t\right) & \text{for } \xi = 0 \\ -\hat{\Gamma}^C\left(\xi\right) : \hat{\tau}\left(\xi, t\right) & \text{for } \xi \neq 0 \end{cases} \tag{31}$$

In the above equation, ξ is the frequency vector and the Fourier transform of an arbitrary field z is denoted by $\hat{z}$. Since the modified Green operator is explicitly known in the frequency domain [40], the convolution product, which reduces to a tensor product, is easily evaluated in the frequency domain. Also, because the polarization field τ depends on the strain field ε, the resolution of the integral equation necessitates an iterative procedure. Different resolution procedures, whose performance depends on the property contrast, have been developed [41, 42, 43]. In the present work, the initial resolution scheme from Moulinec and Suquet [33] is used. For this specific iterative scheme, convergence is met when static equilibrium conditions are fulfilled according to a certain tolerance e':

$$\frac{\sqrt{< ||\nabla_x \cdot \sigma||^2 >_V}}{||\Sigma||} \leq e' \tag{32}$$

Once convergence has been reached, the inverse Fourier transform is applied to express the strain field in the spatial domain.

2.4. Self-consistent method

While the finite element and spectral methods provide numerical solutions to the heterogeneous problem, the solution calculated with the self-consistent method is an approximation. This approximation is obtained by considering

the volume element as an infinite medium with homogeneous strain rate boundary conditions for which the velocity field on ∂V depends on the prescribed macroscopic strain rate:

$$\dot{u} = \dot{E} \cdot x \tag{33}$$

For heterogeneous materials with an elastic-viscoplastic behavior, different approaches have been developed (e.g. [12, 13, 15, 16]). In the present work, the self-consistent model recently developed by Mareau and Berbenni [20] is considered. This model is based upon an affine linearization procedure of the viscoplastic flow rule:

$$\dot{\varepsilon}_p(x,t) \approx m(x,t) : \sigma(x,t) + \dot{\eta}(x,t) \tag{34}$$

m (with $b = m^{-1}$) is the viscoplastic compliance tensor whose definition is:

$$m = \frac{\partial f}{\partial \sigma} \tag{35}$$

$\dot{\eta}$ is the back-extrapolated viscoplastic strain rate:

$$\dot{\eta} = \dot{\varepsilon}_p - m : \sigma \tag{36}$$

The constitutive model (11) is therefore re-written in the following form:

$$\dot{\sigma} = c : (\dot{\varepsilon} - m : \sigma - \dot{\eta}) \tag{37}$$

In the model of Mareau and Berbenni [20], a specific form of the integral equation is derived by introducing fluctuations (δc and δb) for both the elastic and viscoplastic moduli:

$$c(x) = C + \delta c(x) \tag{38}$$

$$b(x) = B + \delta b(x) \tag{39}$$

where C and B are the moduli associated with the elastic and viscoplastic reference media. The corresponding modified Green operators Γ^C and Γ^B are now introduced in the constitutive relation (37) to obtain the integral equation. Using the specific properties of the modified Green operators Γ^B and Γ^C, given by relations (28) and (29), leads to:

$$\dot{\varepsilon} = \dot{E} - \Gamma^C * (\delta c : \dot{\varepsilon}_e) - \Gamma^B * (\delta b : \dot{\varepsilon}_p - b : \dot{\eta}) + \left(\Gamma^C : C - \Gamma^B : B\right) * \dot{\varepsilon}_p \tag{40}$$

The above integral equation, which contains the entire heterogeneous problem, shows how the local strain rate depends on both the macroscopic strain rate and the interactions between the different points of the representative volume element. The self-consistent approximation aims at finding an estimate of the local strain rate, stress rate and stress fields. The estimate is based upon the decomposition of the modified Green tensors into local (subscript l) and non-local (subscript nl) parts:

$$\Gamma^C(x - x') = \Gamma^C_l \delta(x - x') + \Gamma^C_{nl}(x - x') \tag{41}$$

$$\Gamma^B(x-x') = \Gamma_l^B \delta(x-x') + \Gamma_{nl}^B(x-x') \tag{42}$$

According to the above decomposition, the integral equation can be divided into local and non-local terms. While the computation of non-local terms is generally not trivial, local terms, which do not involve any convolution operation, are easily evaluated. However, special attention must be paid to neglect non-local terms without compromising the description of the interactions associated with the elastic-viscoplastic coupling. One possible way consists of solving independently the integral equations obtained for the same representative volume element with either a purely elastic or a purely viscoplastic behavior. Indeed, for the specific cases of pure elasticity and pure viscoplasticity, the constitutive relation (37) takes a simple affine form. For heterogeneous problems with such constitutive equations, estimates of the unknown strain rate fields may be obtained from the self-consistent approximation:

$$\dot{\varepsilon} = A^{Ce} : \dot{E} \text{ for pure elasticity} \tag{43}$$

$$\dot{\varepsilon} = A^{Be} : \dot{E} + A^{Be} : \Gamma_l^{Be} : \left(b : \dot{\eta} - B^e : \dot{N}^e\right) \text{ for pure viscoplasticity} \tag{44}$$

A^{Ce} and A^{Be} are the strain rate localization tensors defined by:

$$A^{Ce} = \left(I + \Gamma_l^{Ce} : (c - C^e)\right)^{-1} \tag{45}$$

$$A^{Be} = \left(I + \Gamma_l^{Be} : (b - B^e)\right)^{-1} \tag{46}$$

with I the fourth rank identity tensor. The effective elastic and viscoplastic moduli tensors C^e (with $S^e = C^{e-1}$) and B^e (with $M^e = B^{e-1}$) are given by:

$$C^e = < c : A^{Ce} >_V \tag{47}$$

$$B^e = < b : A^{Be} >_V \tag{48}$$

For the heterogeneous medium with a purely viscoplastic behavior, the effective back-extrapolated strain rate is:

$$\dot{N}^e = \Gamma_l^{Be^{-1}} : M^e :< A^{Be} : b : \Gamma_l^{Be} : \dot{\eta} >_V \tag{49}$$

In the approach of Mareau and Berbenni [20], the self-consistent solutions obtained for the purely elastic and purely viscoplastic heterogeneous problems are combined using translated field techniques to deduce the final strain rate localization rule:

$$\begin{aligned}
\dot{\varepsilon} = {} & A^{Ce} : \dot{E} + A^{Ce} : \Gamma_l^{Be} : \left(b : \dot{\eta} - B^e : \dot{N}^e\right) \\
& + A^{Ce} : \Gamma_l^{Ce} : \left(\delta c : \dot{\varepsilon}^p + c : A^{Ce} : \left(< \dot{\varepsilon}_p > - \dot{E}_p^e\right)\right) \\
& - A^{Ce} : \Gamma_l^{Be} : \left(\delta b : \dot{\varepsilon}^p - b : A^{Be} : \left(M^e : \Sigma + \dot{N}^e - < \dot{\varepsilon}_p >\right)\right) \\
& + A^{Ce} : \left(\Gamma_l^{Ce} : C^e - \Gamma_l^{Be} : B^e\right) : \left(\dot{\varepsilon}_{vp} - A^B :< \dot{\varepsilon}_p >\right) \\
& - A^{Ce} : \left(\Gamma_l^{Ce} : C^e - \Gamma_l^{Be} : B^e\right) : \left(A^{Be} : \Gamma_l^{Be} : \left(b : \dot{\eta} - B^e : \dot{N}^e\right)\right)
\end{aligned} \tag{50}$$

The localization relation (50) shows how the local strain rate $\dot{\varepsilon}$ depends on both the boundary conditions $\dot{E}$ and the interactions resulting from the elastic and viscoplastic incompatibilities. From a numerical point of view, the implementation of the present approach is relatively straight forward since only the self-consistent solutions of the purely elastic and purely viscoplastic heterogeneous problems are required for the calculation of the strain rate field. In the above relation, $\dot{E}_p^e$ is the effective viscoplastic strain rate which is chosen to impose the averaging condition:

$$\dot{\Sigma} =< \dot{\sigma} >_V \tag{51}$$

3. Results

3.1. Constitutive model and material parameters

For polycrystalline materials, the local behavior of each crystal is largely impacted by its orientation because of the anisotropy of elastic and plastic properties. In the present work, the local behavior is described within a crystal plasticity framework using the constitutive relations proposed by Méric and Cailletaud [44]. The constitutive relations are specified for each slip system s which is uniquely defined from two unitary vectors: the slip plane normal n^s and the slip direction b^s. Thus, considering a crystal with N slip systems (i.e. $s = 1$ to N), the constitutive model is described from equations (52) to (56):

$$\dot{\varepsilon}_p = \sum_{s=1}^{N} \frac{1}{2} \left(n^s \otimes b^s + b^s \otimes n^s \right) \dot{\gamma}^s \tag{52}$$

$$\dot{\gamma}^s = \left(\frac{\langle |\tau^s - x^s| - r^s \rangle}{K} \right)^m \operatorname{sign} \left(\tau^s - x^s \right) \tag{53}$$

$$\tau^s = \sigma : \left(b^s \otimes n^s \right) \tag{54}$$

$$x^s = A y^s \text{ with } \dot{y}^s = \dot{\gamma}^s - D y^s |\dot{\gamma}^s| \tag{55}$$

$$r^s = r_0 + \sum_{t=1}^{N} Q H^{st} q^t \text{ with } \dot{q}^t = \left(1 - B q^t \right) |\dot{\gamma}^t| \tag{56}$$

According to this constitutive model, the viscoplastic shear strain rate $\dot{\gamma}^s$ for the slip system s depends on:

- the resolved shear stress τ^s which is related to the stress tensor σ through the Schmid law,
- the isotropic hardening shear stress r^s which is related to the internal variable q^s,
- the kinematic hardening shear stress x^s which is related to the internal variable y^s.

c_{1111} (GPa)	c_{1122} (GPa)	c_{1212} (GPa)	K (MPa)	m	
197	125	122	12	11	
r_0 (MPa)	Q (MPa)	B	a (MPa)	d	
40	10	3	40 000	1500	
h_1	h_2	h_3	h_4	h_5	h_6
1	1	0.6	12.3	1.6	1.8

Table 1: Material parameters for the 316L stainless steel polycrystalline aggregates [45]. Only independent elastic constants and non-zero coefficients are indicated.

Different material parameters have been introduced in the constitutive model: K is a viscosity parameter, m is a strain rate sensitivity parameter, A and D are kinematic hardening parameters and Q, B and H are isotropic hardening parameters.

According to this constitutive model, the local intrinsic dissipation source d_1 is given by:

$$d_1 = \sigma : \dot{\varepsilon}_p - \sum_{s=1}^{N} x^s \dot{y}^s - \sum_{s=1}^{N} \left(r^s - r_0\right) \dot{q}^s \tag{57}$$

At time t, the local dissipated energy density w_d is thus obtained from:

$$w_d = \int_0^t d_1 dt' \tag{58}$$

The material properties given in table 1 are used for the different simulations. They have been determined for 316L by Guilhem et al. [45]. Only the $\{111\} < 110 >$ plastic slip systems are considered. The matrix H, which is a $N \times N$ matrix describing the interactions between the different slip systems, is defined from six constants (h_1 to h_6). As initially proposed by Hirth [46], the constants correspond to different types of interactions between a given slip system and the other systems. For two slip systems (say s and t), the interaction term H^{st} depends whether the systems are identical ($H^{st} = H^{ss} = h_1$), coplanar ($H^{st} = h_2$), collinear ($H^{st} = h_3$), Hirth junction ($H^{st} = h_4$), forming glissile junction ($H^{st} = h_5$) or forming sessile junction ($H^{st} = h_6$).

3.2. Representative volume elements

For the present comparison, ten different polycrystalline aggregates are considered. Each aggregate consists of two hundred equiaxed grains that were built from a periodic Voronoï tessellation. To obtain regular polyhedrons, germ positions were fixed according to an iterative procedure which imposes a minimal distance between two germs [47]. Also, small edges were removed to ensure a sufficient quality of the finite element mesh. The set of crystallographic orientations was selected using the discretization technique proposed by Melchior and Delannay [48] to represent as better as possible a random texture. It is emphasized that the same set of orientations is used for each aggregate. It is

therefore possible to define some average quantities for each grain (the total number of grains is $2000 = 10 \times 200$), for each orientation (the total number of orientations is 200), for each aggregate (the total number of aggregates is 10) or for the whole set of aggregates.

For self-consistent calculations, the different grains of the representative volume element are treated as spherical inclusions embedded in a homogeneous medium. For the application of the spectral method, the 3D microstructure is discretized into $128 \times 128 \times 128 \approx 2,000,000$ voxels (see figure 1). For finite element simulations, the microstructure is represented with approximately 200,000 tetrahedral elements with a quadratic interpolation of the displacement field (see figure 1). For a such resolution, the total number of degrees of freedom for the finite element problem is about 1,000,000.

To determine whether convergence is achieved or not, the spectral and finite element methods involve numerical tolerances. In the present work, the numerical tolerances e and e' were respectively set to 10^{-4} and 10^{-5}. With a further reduction of these tolerances, the different components of the local stress and strain tensors are not altered up to the fourth significant digit. A detailed investigation of the influence of these tolerances has been carried out by Eisenlohr et al. [37].

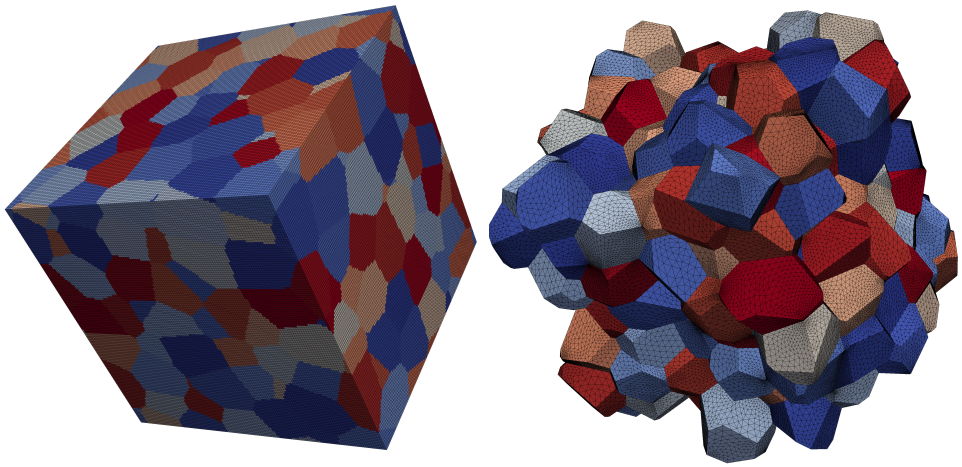

Figure 1: Discretization of the periodic representative volume elements used for the present comparison. The grid used for performing calculations with the spectral method is plotted on the left side. The mesh used for performing calculations with the finite element method is plotted on the right side.

3.3. Computing facilities and softwares

The numerical implementation of the self-consistent, spectral and finite element methods has been done by the authors. The different methods use exactly

Method	Strain rate (s^{-1})	Young's modulus (GPa)	Yield stress (MPa)	Strain hardening exponent
FEM	0.005	191.4	182	0.049
	0.05		186	0.048
	0.5		192	0.047
FFT	0.005	191.1	181	0.039
	0.05		185	0.039
	0.5		190	0.038
SC	0.005	191.3	179	0.064
	0.05		184	0.062
	0.5		191	0.060

Table 2: Effective properties determined with different methods in the case of uniaxial tension for different strain rates 0.005 s^{-1}, 0.05 s^{-1} and 0.5 s^{-1}.

the same numerical procedure for the integration of the constitutive model (a semi-implicit time integration scheme). The implementation of the spectral method is based upon the FFTW algorithm proposed by Frigo and Johnson [49]. For the finite element method, the resolution of the linear system of equations is achieved with the MUMPS solver [50]. Both the finite element and spectral methods make an intensive use of shared-memory parallel programming. The self-consistent method is entirely implemented in a sequential mode. The calculations were performed on a DELL PowerEdge R710 server with 2 processors (Intel Xeon X5690) with 6 cores each and with 96 GB of RAM. For the spectral and finite element methods, mesh or grid refinements are generally limited by computation times.

3.4. Uniaxial tension

The case of uniaxial tension, up to a macroscopic strain E_{11} of 5%, is first examined. Different strain rate conditions are imposed to the polycrystalline aggregates: 0.005 s^{-1}, 0.05 s^{-1} and 0.5 s^{-1}. The results obtained from the finite element (labeled as FEM), spectral (labeled as FFT) and self-consistent (labeled as SC) methods are plotted in figure 2. The effective values of the Young's modulus, the 0.2% offset yield stress and the strain hardening exponent determined with the different methods are given in table 2.

According to the Young's modulus and yield stress estimates, no significant difference is observed between the different methods within the elastic regime. However, as shown by the different strain hardening exponents, some discrepancies exist within the plastic regime. The explanation for these differences is twofold. First, the effective properties calculated with the self-consistent method result from an approximation of the integral equation (40) associated with the heterogeneous problem. Therefore, the overestimation of the strain hardening exponent with the self-consistent method is caused by the neglecting

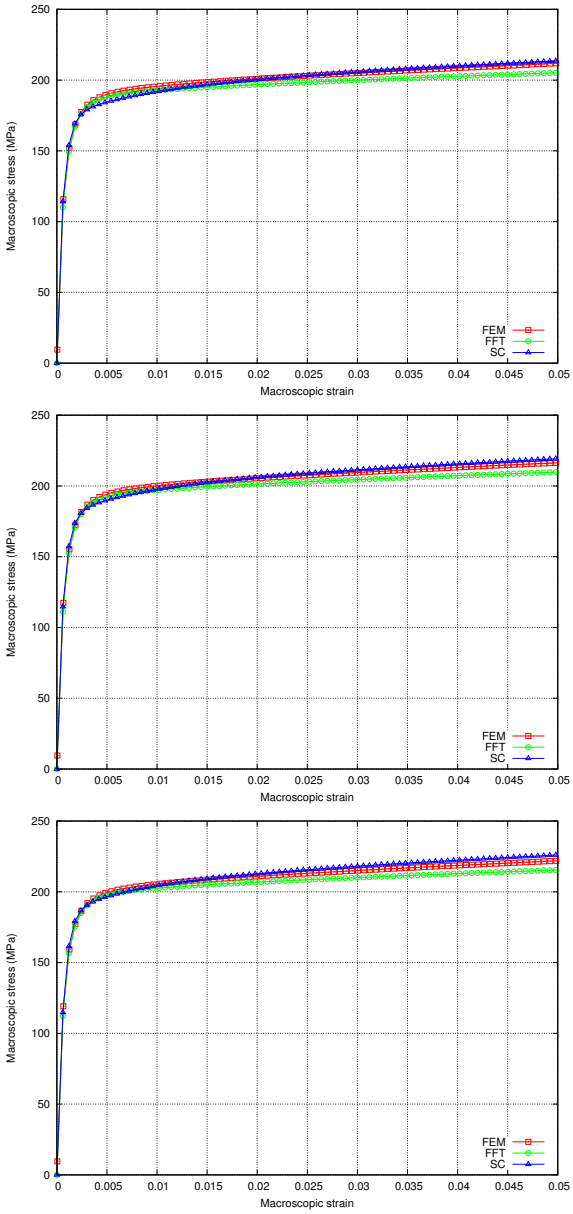

Figure 2: Evolution of the macroscopic stress as a function of the macroscopic strain determined with different methods in the case of uniaxial tension for different strain rates 0.005 s^{-1} (top), 0.05 s^{-1} (middle) and 0.5 s^{-1} (bottom).

of non-local contributions which appear in the integral equation. Also, the finite element and spectral methods consider the entire heterogeneous problem so

similar values of the strain hardening exponent should be obtained with these numerical methods. However, the accuracy of these methods is conditioned by the mesh/grid resolution used for discretizing the representative volume elements. In order to evaluate spatial convergence, the axial stress Σ_{11} obtained at the end of uniaxial tension simulations (i.e. when $E_{11} = 0.05$) has been computed with different mesh/grid resolutions for a macroscopic strain rate of 0.05 s^{-1}. As illustrated by figure 3, the resolution used for performing calculations with the spectral method (i.e. 2,000,000 voxels) is such that further refinement does not significantly alter the macroscopic mechanical response. For finite element calculations, the final axial stress is found to change importantly with an increasing mesh resolution. As a consequence, since further mesh refinement is practically not possible with the available computing facilities, convergence cannot be guaranteed for finite element calculations with 1,000,000 degrees of freedom.

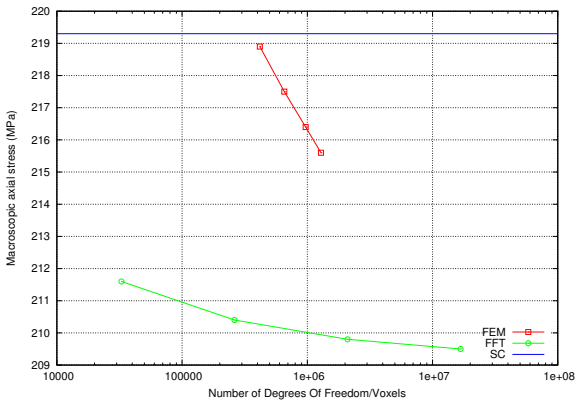

Figure 3: Evolution of the macroscopic axial stress obtained at the end of uniaxial tension simulations for a macrocopic strain rate of 0.05 s^{-1} as a function of the mesh/grid resolution. Since the self-consistent method does not require any spatial discretization, the results are independent of the spatial resolution.

The evolution of the yield stress as a function of the strain rate, which provides some information regarding the effective strain rate sensitivity of the polycrystalline aggregates, is plotted in figure 4. While the effective strain rate sensitivities obtained from the spectral and finite element methods are very similar, the polycrystalline aggregates display a slightly higher strain rate sensitivity according to the self-consistent method.

Figure 5 shows the evolution of the computation time needed for calculating the response of a polycrystalline aggregate under uniaxial tension according to the self-consistent, spectral and finite element methods as a function of the mesh/grid resolution. In comparison with full field methods, the self-consistent method necessitates very low computational resources while it provides a reasonable description of the macroscopic behavior. Also, in contrast with the spectral method, the finite element method is rapidly limited by the computation time

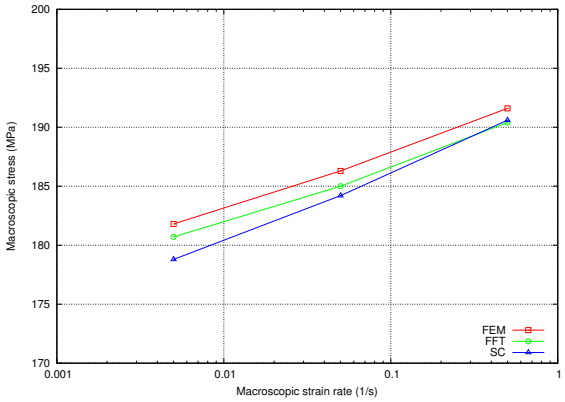

Figure 4: Evolution of the 0,2% offset yield stress as a function of the macroscopic strain rate determined from different methods in the case of uniaxial tension.

which is important for fine mesh resolutions.

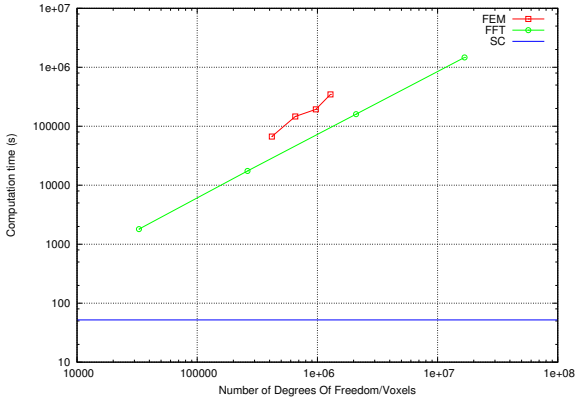

Figure 5: Evolution of the computation time needed for calculating the response of the polycrystalline aggregate under uniaxial tension according to the self-consistent, spectral and finite element methods as a function of the mesh/grid resolution. Since the self-consistent method does not require any spatial discretization, the results are independent of the spatial resolution.

3.5. Cyclic plasticity

The case of cyclic plasticity is now considered. Different uniaxial strain-controlled cyclic tests are simulated with the finite element, spectral and self-consistent methods. Simulations are performed with a loading frequency of 1 Hz and with strain amplitudes of 0.4% and 0.8%. The results obtained for the 10th loading cycle are plotted in figure 6. No major difference is observed between the different methods for both strain amplitudes.

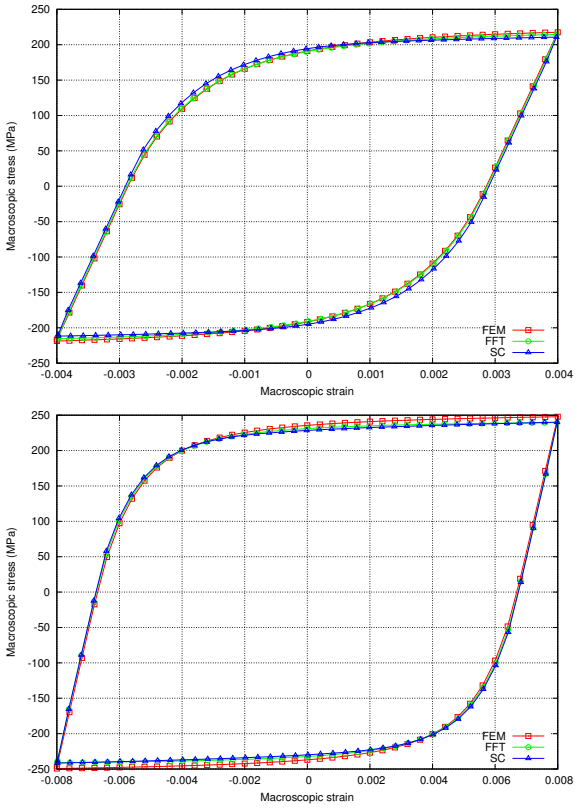

Figure 6: Evolution of the macroscopic stress as a function of the macroscopic strain determined with different methods in the case of cyclic plasticity for different strain amplitudes: 0.4% (top) and 0.8% (bottom).

To observe possible discrepancies between the different methods at the local scale, the average axial stress $< \sigma_{11} >_{V_g}$, the average axial strain $< \varepsilon_{11} >_{V_g}$ and the average dissipated energy density $< w_d >_{V_g}$ are determined for each grain g with volume V_g. Figure 7 shows the cumulative distribution functions obtained for these quantities according to the different methods at the end of the last cycle for both strain amplitudes (when $E_{11} = -0.8\%$ or -0.4%). Though the distributions obtained from the spectral and finite element methods are quite similar, internal stresses are found to be overestimated by the finite element method for which, because of the insufficient mesh resolution, the fulfillment of local equilibrium conditions is not guaranteed. Also, the results calculated from the self-consistent method are much less scattered than those determined with the other methods. However, by design, the self-consistent model does not provide any information about the state of a specific grain. The influence of neighboring grains is not explicitly accounted for with the self-consistent method which, strictly speaking, allows for determining the average response of a group

of grains having identical features (e.g. orientation, shape).

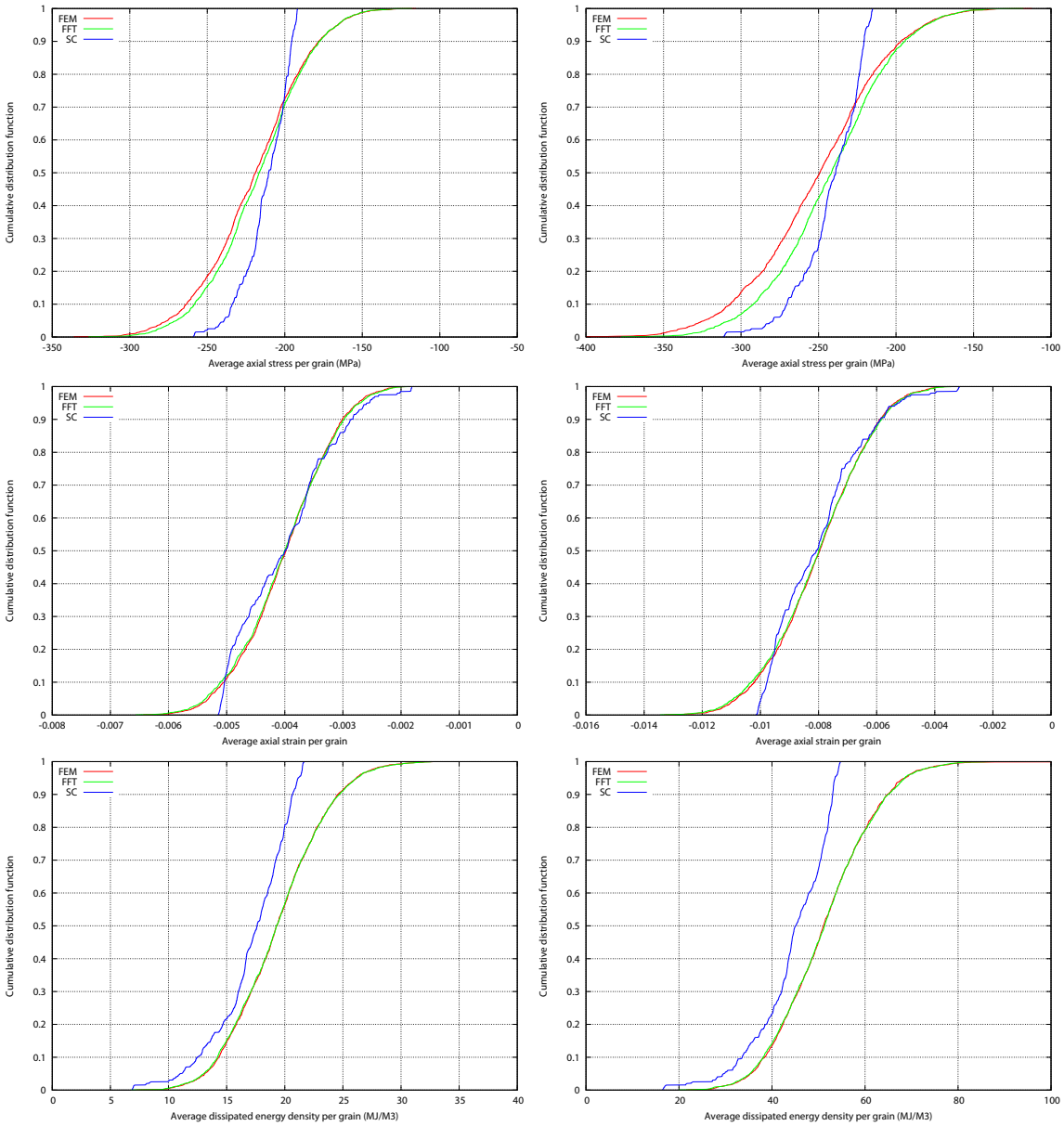

Figure 7: Cumulative distribution functions obtained for the average axial stress (top), the average axial strain (middle) and the average dissipated energy (bottom) per grain at the end of the last cycle for different macroscopic strain amplitudes: 0.4% (left) and 0.8% (right).

An alternative point of view thus consists of comparing some average quantities per orientation. Figure 8 shows the cumulative distribution functions ob-

tained for the average axial stress $< \sigma_{11} >_{V_c}$, the average axial strain $< \varepsilon_{11} >_{V_c}$ and the average dissipated energy density $< w_d >_{V_c}$ per orientation. Such quantities have been computed for each crystallographic orientation c with volume V_c at the end of the last cycle for both strain amplitudes. According to figure 8, for the average axial stress and axial strain per orientation, the cumulative distribution functions obtained with the self-consistent, spectral and finite element methods are in reasonable agreement. More specifically, though the self-consistent method is not appropriate for determining the state of a specific grain, it provides correct estimates of the average stress-strain response of a given orientation (i.e. a group of grains with identical features). However, when looking at the average dissipated energy density per orientation, important discrepancies exist between the self-consistent method and the full field methods. Indeed, because the dissipation source is a highly non-linear function of the stress state, small discrepancies regarding the local stress state propagate into important differences regarding the dissipated energy density.

3.6. Yield surface

To correctly model the behavior of a polycrystalline aggregate submitted to multiaxial loading conditions, an accurate description of the yield surface is generally required. In this section, the yield surfaces obtained from the finite element, spectral and self-consistent methods are compared for various prestraining conditions: without any prestraining, after a uniaxial tension prestraining up to a macroscopic strain E_{11} of 5% and after a shear prestraining up to a macroscopic strain E_{12} of 5%. The yield surfaces are determined from different stress-controlled monotonic loadings resulting from combinations of normal stresses and shear stresses (Σ_{11} and Σ_{12}). The onset of plastic yielding is detected using a 0.1% offset equivalent plastic strain criterion.

As shown by figure 9, the results determined with the different methods are in good agreement with each other. More specifically, the evolution of the yield surface is mostly governed by kinematic hardening since a significant translation of the yield surface, rather than a large expansion, is observed when a prestraining is applied to polycrystalline aggregates. Therefore, though some discrepancies may exist regarding the evolution of internal stresses, the impact of internal stresses on the effective macroscopic behavior is correctly described by the different methods.

4. Conclusions

In the present work, different methods for the determination of the effective properties of polycrystalline aggregates with an elastic-viscoplastic behavior have been compared. First, the main features of the finite element, spectral and self-consistent methods have been briefly recalled. Using a crystal plasticity based constitutive model, the effective behavior of different 316L polycrystalline aggregates has been determined with the different methods. The responses have

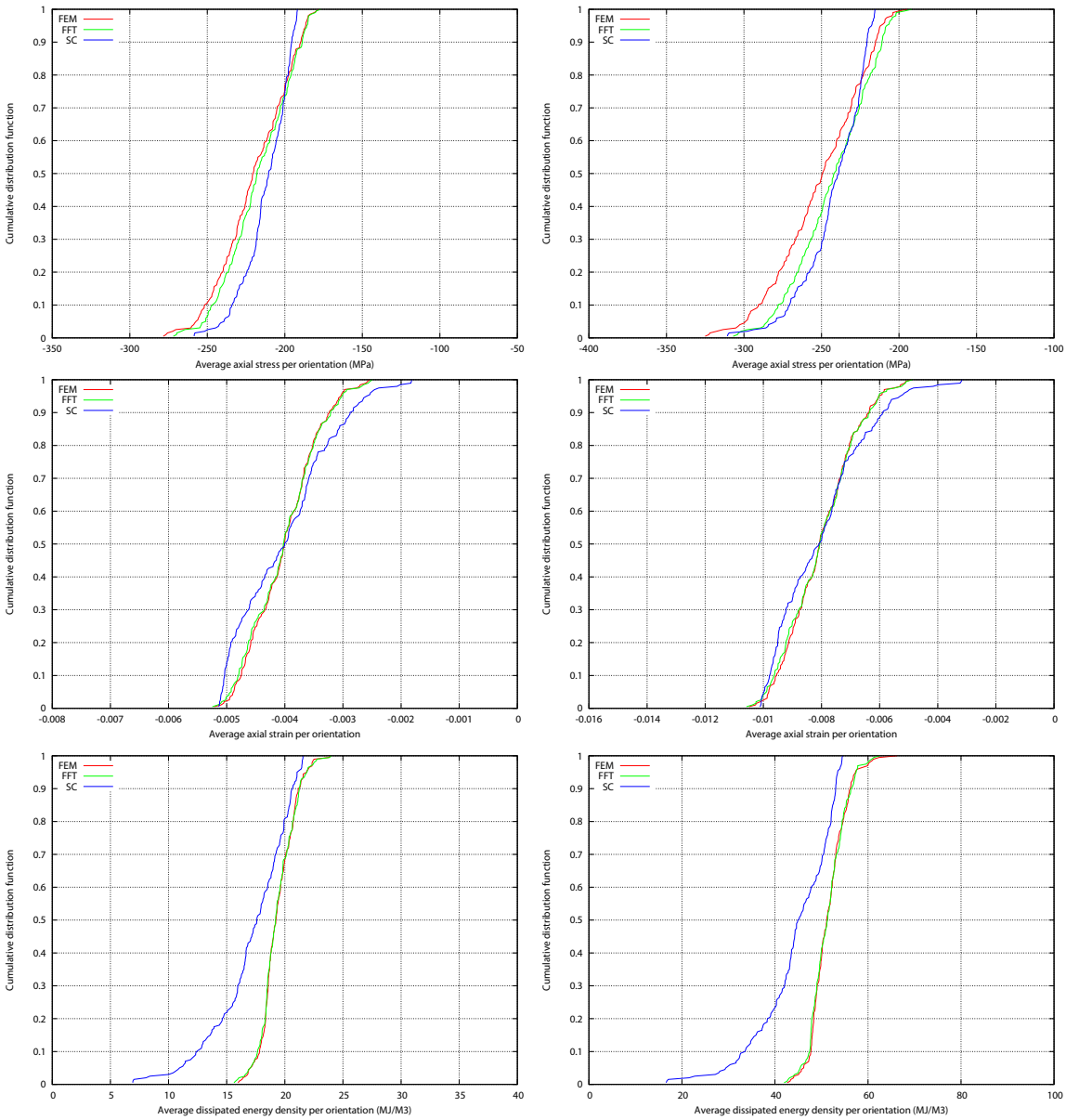

Figure 8: Cumulative distribution functions obtained for the average axial stress (top), the average axial strain (middle) and the average dissipated energy (bottom) per orientation at the end of the last cycle for different macroscopic strain amplitudes: 0.4% (left) and 0.8% (right).

been computed for various loading conditions: uniaxial tension, cyclic tension-compression and different loading paths allowing for the determination of yield

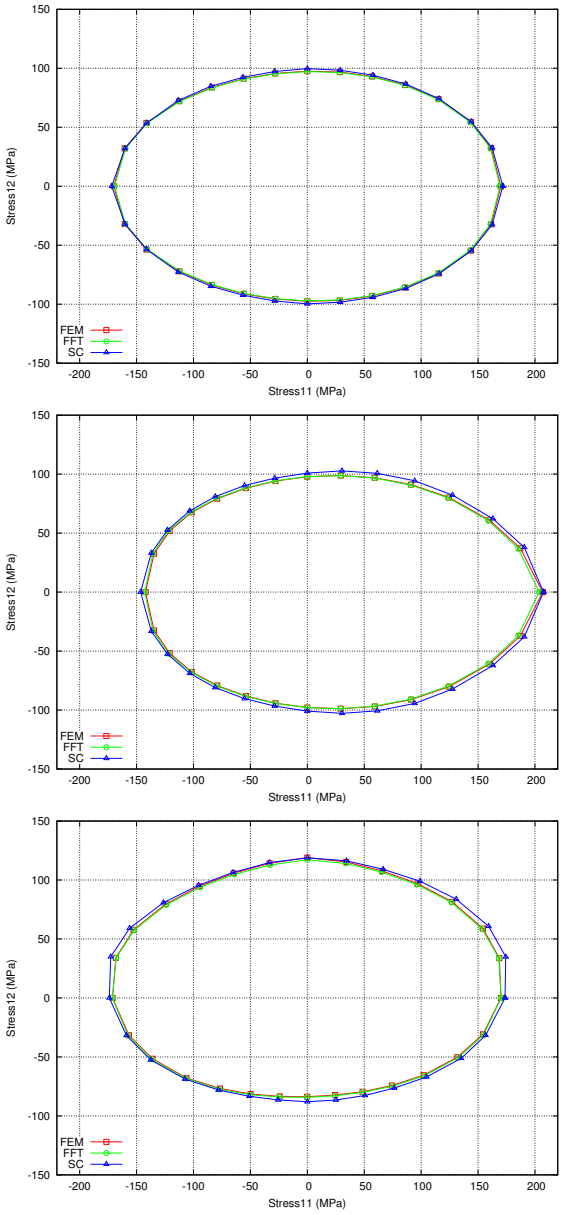

Figure 9: Yield surfaces determined with different methods for a 316L polycrystalline aggregates for various prestraining conditions: without any prestraining (top), after a uniaxial tension prestraining up to a macroscopic strain E_{11} of 5% (middle) and after a shear prestraining up to a macroscopic strain E_{12} of 5% (bottom).

surfaces.

When looking at the macroscopic behavior, no major difference is observed

between the different methods. However, though similar results should be obtained with the finite element and spectral methods, the hardening rate is found to be slightly overestimated by the finite element method. Indeed, the accuracy of the finite element and spectral methods is conditioned by the mesh/grid resolution used for discretizing the representative volume element. As shown by the results obtained for uniaxial tension, spatial convergence cannot be guaranteed for finite element calculations. A particular care must thus be taken when using the finite element method for estimating effective properties. Fine mesh resolutions, for which the computational cost is possibly high, might be needed to get accurate estimates.

The observation of the local behavior shows important discrepancies between the self-consistent method and the other methods. Indeed, since the self-consistent method underestimates the influence of neighboring grains, it is not appropriate for determining the mechanical response of a specific grain. Nevertheless, when looking at either the macroscopic response or the average response of a group of grains with identical features, the self-consistent method is found to provide correct estimates within short computation times.

[1] A.V. Hershey, The elasticity of an isotropic aggregate of anisotropic cubic crystals, ASME, Journal of Applied Mechanics 21 (1954) 236–240.

[2] E. Kröner, Berechnung der elastischen Konstanten des Vielkristalls aus den konstanten des Einskristalls, Zeitschrift fur Physik 151 (1958) 504.

[3] E. Kröner, Zur plastischen Verformung des Vielkristalls, Acta Metallurgica 9 (1961) 155–161.

[4] R. Hill, Continuum micro-mechanics of elastoplastic polycrystals, Journal of the Mechanics and Physics of Solids 13 (1965) 89–101.

[5] J.W. Hutchinson, Bounds and self-consistent estimates for creep of polycrystalline materials, Proceedings of the Royal Society of London A 348 (1976) 101–127.

[6] A. Molinari, G.R. Canova, S. Ahzi, A self consistent approach of the large deformation polycrystal viscoplasticity, Acta Metallurgica 35 (1987) 2983–2994.

[7] R.A. Lebensohn, C.N. Tomé, A self-consistent anisotropic approach for the simulation of plastic deformation and texture development of polycrystals: Application to zirconium alloys, Acta Metallurgica et Materialia 41 (1993) 2611–2624.

[8] Suquet, P., Elements of homogenization for inelastic solid mechanics, in: E. Sanchez-Palencia, A. Zaoui (Eds.), Homogenization Techniques for Composite Media, Lecture Notes in Physics vol. 272, Springer, New York, 1987, pp. 193–278.

[9] Z. Hashin, The inelastic inclusion problem, International Journal of Engineering Science 7 (1969) 11-36.

[10] N. Laws, R. McLaughlin, Self-consistent estimates for the viscoelastic creep compliances of composite materials, Proceedings of the Royal Society of London A 359 (1978) 251–273.

[11] Y. Rougier, C. Stolz, A. Zaoui, Self-consistent modelling of elasticviscoplastic polycrystals, Comptes Rendus Academie des Sciences Paris 318 (1994) 145–51.

[12] R. Masson, A. Zaoui, Self-consistent estimates for the rate-dependent elastoplastic behaviour of polycrystalline materials, Journal of the Mechanics and Physics of Solids 47 (1999) 1543–1568.

[13] G.J. Weng, Self-consistent determination of time-dependent behavior of metals. ASME, Journal of Applied Mechanics 48 (2001) 41–46.

[14] S. Nemat-Nasser, M., Obata, Rate-dependent, finite elasto-plastic deformation of polycrystals, Proceedings of The Royal Society of London A 407 (1986) 343–375.

[15] A. Paquin, H. Sabar, M. Berveiller, Integral formulation and self-consistent modelling of elastoviscoplastic behavior of heterogeneous materials, Archive of Applied Mechanics 69 (1999) 14–35.

[16] H. Sabar, M. Berveiller, V. Favier, S. Berbenni, A new class of micromacro models for elasticviscoplastic heterogeneous materials, International Journal of Solids and Structures 39 (2002) 3257–3276.

[17] N. Lahellec, P. Suquet, Effective behavior of linear viscoelastic composites: A time-integration approach, International Journal of Solids and Structures 44 (2007) 507–529.

[18] S. Mercier, A. Molinari, A., Homogenization of elasticviscoplastic heterogeneous materials: Self-consistent and Mori-Tanaka schemes, International Journal of Plasticity 25 (2009) 1024–1048.

[19] H. Wang, P.D. Wu, C.N. Tomé, Y. Huang, A finite strain elastic-viscoplastic self-consistent model for polycrystalline materials, Journal of the Mechanics and Physics of Solids 58 (2010) 594–612.

[20] C. Mareau, S. Berbenni, An affine formulation for the self-consistent modeling of elasto-viscoplastic heterogeneous materials based on the translated field method, International Journal of Plasticity 64 (2015) 134–150.

[21] M.J. Turner, R.W. Clough, C.H. Martin, L.J. Topp, Stiffness and deflection analysis of complex structures, J. Aero. Sci. 23 (1956) 805–824.

[22] O.C. Zienkiewicz, Y.K. Cheung, Finite elements in the solution of field problems, The Engineer (1965) 507–510.

[23] O. Zienkiewicz, The Finite Element Method in Structural and Continuum Mechanics, McGraw-Hill, New York, 1967.

[24] H. Miyamoto, M. Sumikawa, T. Miyoshi, Interpretation of mechanical behavior of pure aluminum in terms of microstructures, in: The 1971 Conference on Mechanical Behavior of Materials, 1972, pp. 140–151.

[25] G.B. Sarma, P.R. Dawson, Texture predictions using a polycrystal plasticity model incorporating neighbor interactions, Int J Plast 12 (1996) 1023–54.

[26] D.P. Mika, P.R. Dawson, Polycrystal plasticity modeling of intracrystalline boundary textures, Acta Mater 47 (1999) 1355–69.

[27] S.R. Kalidindi, Modeling anisotropic strain hardening and deformation textures in low stacking fault energy fcc metals, Int J Plast 17 (2001) 837–60.

[28] F. Barbe, L. Decker, D. Jeulin, G. Cailletaud, Intergranular and intragranular behavior of polycrystalline aggregates. Part 1: F.E. model, Int J Plast 17 (2001) 513–36.

[29] F. Barbe, S. Forest, G. Cailletaud, Intergranular and intragranular behavior of polycrystalline aggregates. Part 2: results, Int. J. Plasticity 17 (2001) 537–563.

[30] O. Diard, S. Leclercq, G. Rousselier, G. Cailletaud, Evaluation of finite element based analysis of 3D multicrystalline aggregates plasticity: Application to crystal plasticity model identification and the study of stress and strain fields near grain boundaries, International Journal of Plasticity 21 (2005) 691–722.

[31] F. Roters, H.S. Jeon-Haurand, D. Raabe, A texture evolution study using the texture component crystal plasticity FEM, Mater Sci Forum 495–497 (2005) 937–44.

[32] H. Abdolvand, M.R. Daymond, C. Mareau, Incorporation of twinning into a crystal plasticity finite element model: Evolution of lattice strains and texture in Zircaloy-2, International Journal of Plasticity 27 (2011) 1721–1738.

[33] H. Moulinec, P. Suquet, A numerical method for computing the overall response of nonlinear composites with complex microstructure, Computer Methods in Applied Mechanics and Engineering 157 (1998) 69–94.

[34] R.A. Lebensohn, N-site modeling of a 3D viscoplastic polycrystal using Fast Fourier Transform, Acta Materialia 49 (2001) 2723-2737.

[35] R.A. Lebensohn, A.K. Kanjarla, P. Eisenlohr, An elasto-viscoplastic formulation based on fast fourier transforms for the prediction of micromechanical fields in polycrystalline materials, International Journal of Plasticity 32–33 (2012) 59–69.

[36] C. Mareau, D. Cuillerer, F. Morel, Experimental and numerical study of the evolution of stored and dissipated energies in a medium carbon steel under cyclic loading, Mechanics of Materials 60 (2013) 93–106.

[37] P. Eisenlohr, M.Diehl, R.A.Lebensohn, F. Roters, A spectral method solution to crystal elasto-viscoplasticity at finite strains, International Journal of Plasticity 46 (2013) 37–53.

[38] J. Dirrenberger, Effective properties of architectured materials, PhD Thesis (2012), Ecole Nationale Supérieure des Mines de Paris

[39] W.H. Müller, Mathematical versus Experimental Stress Analysis of Inhomogeneities in Solids, J. Phys. IV 6 (1996) 139–148.

[40] T. Mura, Micromechanics of defects in solids, Kluwer Academic Publishers, Dordrecht, The Netherlands, 1987.

[41] D.J. Eyre, G.W., Milton, A fast numerical scheme for computing the response of composites using grid refinement, Journal of Physique III 6 (1999) 41–47.

[42] J.C. Michel, H. Moulinec, P. Suquet, A computational scheme for linear and non-linear composites with arbitrary phase contrast, Int. J. Numer. Meth. Engng 52 (2001) 139–160.

[43] J. Zeman, J. Vondrejc, J. Novák, I. Marek, Accelerating a FFT-based solver for numerical homogenization of periodic media by conjugate gradients, Journal of Computational Physics 229 (2010) 8065–8071.

[44] L. Méric, G. Cailletaud, Single crystal modeling for structural calculations: Part 2 - Finite element implementation, ASME, Journal of Engineering Materials and Technology 113 (1991) 171–182.

[45] Y. Guilhem, S. Basseville, F. Curtit, J.M. Stéphan, G. Cailletaud, Numerical investigations of the free surface effect in three-dimensional polycrystalline aggregates, Computational Materials Science 70 (2013) 150–162.

[46] J.P. Hirth, On dislocation interactions in the FCC lattice, Journal of Applied Physics, 32 (1960) 700–706.

[47] F. Fritzen, T. Böhlke, E. Schnack, Periodic three-dimensional mesh generation for crystalline aggregates based on Voronoi tessellations, Computational Mechanics 43 (2009) 701–713.

[48] M.A. Melchior, L. Delannay, A texture discretization technique adapted to polycrystalline aggregates with non-uniform grain size, Computational Materials Science 37 (2006) 557–564.

[49] M. Frigo, S.G. Johnson, The Design and Implementation of FFTW3, in: Proceedings of the IEEE 93 (2), Special Issue on Program Generation, Optimization, and Platform Adaptation, 2005, 216–231.

[50] E. Agullo, P. Amestoy, A. Buttari, A. Guermouche, G. Joslin, J.-Y. L'Excellent, X.S. Li, A. Napov, F.-H. Rouet, M. Sid-Lakhdar, S. Wang, C. Weisbecker, I. Yamazaki, Recent Advances in Sparse Direct Solvers, in: 22nd Conference on Structural Mechanics in Reactor Technology, San Francisco, 2013.